Cave sediments constrain the latest Pleistocene advance of the Laurentide Ice Sheet in the Champlain Valley, Vermont, USA

JQS
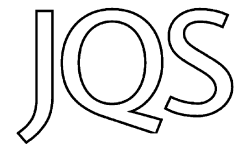
JEFFREY S. MUNROE,* ZACHARY M. PERZAN and WILLIAM H. AMIDON
Geology Department, Middlebury College, Middlebury, VT 05753, USA

ABSTRACT: Optically stimulated luminescence (OSL) and infrared stimulated luminescence (IRSL) dating were applied to cave sediments that were protected from the Marine Isotope Stage 2 (MIS-2) advance of the Laurentide Ice Sheet (LIS) in the Champlain Valley of western Vermont. Evidence indicates that these sediments were derived from a subaerial landscape, requiring that the ice margin was north of the Champlain Valley when they were deposited. A basal sandy gravel was deposited during MIS-4 ($\sim$68 ka), sand near the middle of the composite stratigraphy was deposited during MIS-3 ($\sim$55 ka), and a layer of coarse sand in the stratigraphically highest position was deposited at the onset of MIS-2 ($\sim$35 ka). The youngest age constrains advance of the LIS south of the international border early in MIS-2, and is combined with other available evidence to constrain ice advance rates over the 12 000 years leading up to the Last Glacial Maximum. Rates estimated from limiting ages were relatively slow (25 ma^{-1}) as the ice ascended the adverse slope out of the St. Lawrence Lowland, increased as the margin advanced through the Champlain Valley, perhaps aided by subglacial bed deformation or ice streaming, and were fastest ($\sim$100 ma^{-1}) as the margin approached the terminal moraine position.
Copyright © 2016 John Wiley & Sons, Ltd.

KEYWORDS: cave sediment; ice advance; Last Glacial Maximum; Laurentide Ice Sheet; luminescence dating.

Introduction

The record of past temperate glacier fluctuations is fundamentally biased towards deposits and landforms created at times of maximum advance and subsequent retreat (Gibbons et al., 1984). In contrast, direct records of glacier advance are rare, due to the likelihood of later erosion by overriding ice. This situation, which applies equally for the smallest cirque glaciers and the largest ice sheets, challenges our ability to reconstruct past ice dynamics and understand the climatic drivers that give rise to glaciations.

In North America, a dominant feature of Quaternary climate cycles is the growth and decay of the Laurentide Ice Sheet (LIS). Decades of moraine mapping and glacial geomorphologic observations (Dyke et al., 2002), bolstered by limiting radiocarbon ages (Lowell et al., 1999, 2009), varve chronologies (Ridge and Toll, 1999; Ridge et al., 1999, 2012) and cosmogenic surface-exposure ages (Balco et al., 2002; Balco and Schaefer, 2006; Ullman et al., 2015), have generated a detailed chronology of ice sheet fluctuations starting with the Last Glacial Maximum (LGM) Wisconsinan Glaciation (Clark et al., 2009) and continuing with time-transgressive deglaciation into the Holocene (Carlson et al., 2008). In contrast, terrestrial records of the LIS before the Late Wisconsinan are sparse and fragmentary, due to generally poor exposure and a paucity of chronologic control on older glacial deposits (Mickelson and Colgan, 2003; Ridge, 2004).

A few localities provide exceptions to this situation. For instance, luminescence dating reveals that interbedded tills and proglacial lake sediments near Toronto, Canada, were deposited between the waning stages of the Sangamon Interglacial [Marine Isotope Stage 5 (MIS-5)] and the Middle Wisconsinan (MIS-3) interstadial (Berger and Eyles, 1994). In the St. Lawrence Lowland (hereafter 'SLL') to the east, the Levrard Till is considered evidence of an ice advance during the Early Wisconsinan, MIS-4 (Lamothe et al., 1992). The Chaudière Till in the Appalachian Uplands south of the SLL is

also thought to represent ice advance during the Early Wisconsinan, although initial phases of that advance may have involved icecaps expanding along the international border (Lamothe et al., 1992). Radiocarbon dating of organic-bearing sediment retrieved from boreholes indicates that the SLL was ice-free during the Middle Wisconsinan, requiring that the LIS had retreated to a position farther north in Québec before the MIS-2 advance (Parent et al., 2015). South of the international border numerous localities reveal multiple tills (Koteff and Pessl, 1985), and although some debate remains (e.g. Colgan and Newman, 1999) the degree of weathering atop the stratigraphically older till is more consistent with deposition during the Illinoisan Glaciation (MIS-6), rather than MIS-4 (Oldale and Colman, 1992; Ridge, 2004). Ice-free conditions before MIS-2 are also recorded by pre-Wisconsinan lake sediment in the Adirondack Mountains of New York (Muller et al., 1993) and the White Mountains of northern New Hampshire (Fowler, 1999).

These localities provide valuable information, yet because they are spatially scattered, compromised by erosional unconformities, and rarely limited by absolute ages, firm constraints on the advance of the LIS south of the SLL during the onset of the MIS-2 glaciation are lacking. In a comprehensive review of the glacial history of New England, Ridge (2004) summarizes this situation with the statement 'In the absence of numerical ages there is currently no precise chronology for the first arrival of Late Wisconsinan ice across New England.' This data gap makes it difficult to determine the timing and pace of ice advance, and complicates efforts to link climatic forcing to ice sheet response.

Here we set temporal limits for the position of the southern LIS margin in the Champlain Valley during the Early/Middle Wisconsinan and subsequent MIS-2 advance by applying luminescence dating to cave sediments that were protected from glacial erosion. Our results constrain the MIS-2 advance of the LIS south of the international border, permitting calculation of ice advance rates that can be compared with records of global ice volume (e.g. Lisiecki and Raymo, 2005) and other data from the region.

*Correspondence: J. S. Munroe, as above.
E-mail: jmunroe@middlebury.edu

Regional setting

The north-draining Champlain Valley, which hosts the modern Lake Champlain, is a north–south-trending lowland separating the Adirondack Mountains of New York from the Green Mountains of Vermont (Fig. 1). The valley, with an average width of ~25 km and maximum relief of ~1.7 km, acted as a major conduit for the LIS during the LGM. Erratics and till atop the highest summits (>1900 m a.s.l.) in the northern Appalachians (Goldthwait, 1939; Fowler, 1979) indicate that ice thickness in the valley was in excess of 2 km. During deglaciation, the retreating LIS impeded northward drainage (Fig. 1), creating Glacial Lake Vermont (Chapman, 1937), which persisted until the Pleistocene–Holocene transition (Rayburn et al., 2007).

Weybridge Cave (44.06145°N, 73.20633°W), one of the larger known solution caves in this region, developed in carbonates of the Ordovician Chipman Formation (Quick and Porter, 2010). The cave contains ~450 m of accessible passageways, most of which constitute a single longitudinal trunk ~35 m below the ground surface that is blocked at both ends by plugs of sediment (Fig. 1). The sole entrance to the cave, at an elevation of ~137 m, was submerged beneath Glacial Lake Vermont, which reached an elevation of ~150 m in the central Champlain Valley (Rayburn et al., 2005). As a result the landscape surrounding the cave entrance is mantled by till and proglacial lake sediment. At

some point after Glacial Lake Vermont drained an ephemeral stream penetrated this sediment and began flushing material into the cave system. The narrow joint-controlled passage exploited by this stream provides access to the trunk of the cave (Fig. 1), which has an oval cross-section (~4 m in diameter) indicative of formation under phreatic conditions (Palmer, 1991). Higher passages are floored with erratic cobbles washed in from the sediment surrounding the cave entrance. In contrast, the trunk is partially filled with 2–3 m of fine laminated sediments overlying a coarse sandy gravel.

Sampling strategy

Thorough reconnaissance was conducted in Weybridge Cave to locate exposures of fine-grained sediment appropriate for this study. Outcrops were eroded by water flowing through the cave at some point in the past, although none are affected by flowing water today. Pre-existing outcrops were utilized to reduce digging-related impacts on the cave environment. Four outcrops were studied and sampled (Fig. 1). At three of these locations, vertical faces were scraped clean with a blade, after which polyethylene U-channels (61 cm long × 2.8 cm wide × 1.9 cm deep) were pounded into the exposure with a mallet, excavated and returned to the laboratory (Fig. 2). The fourth outcrop (Outcrop E, Fig. 1) was too short to sample with a U-channel. Instead, the stratigraphy was described and sampled in situ. In the laboratory the
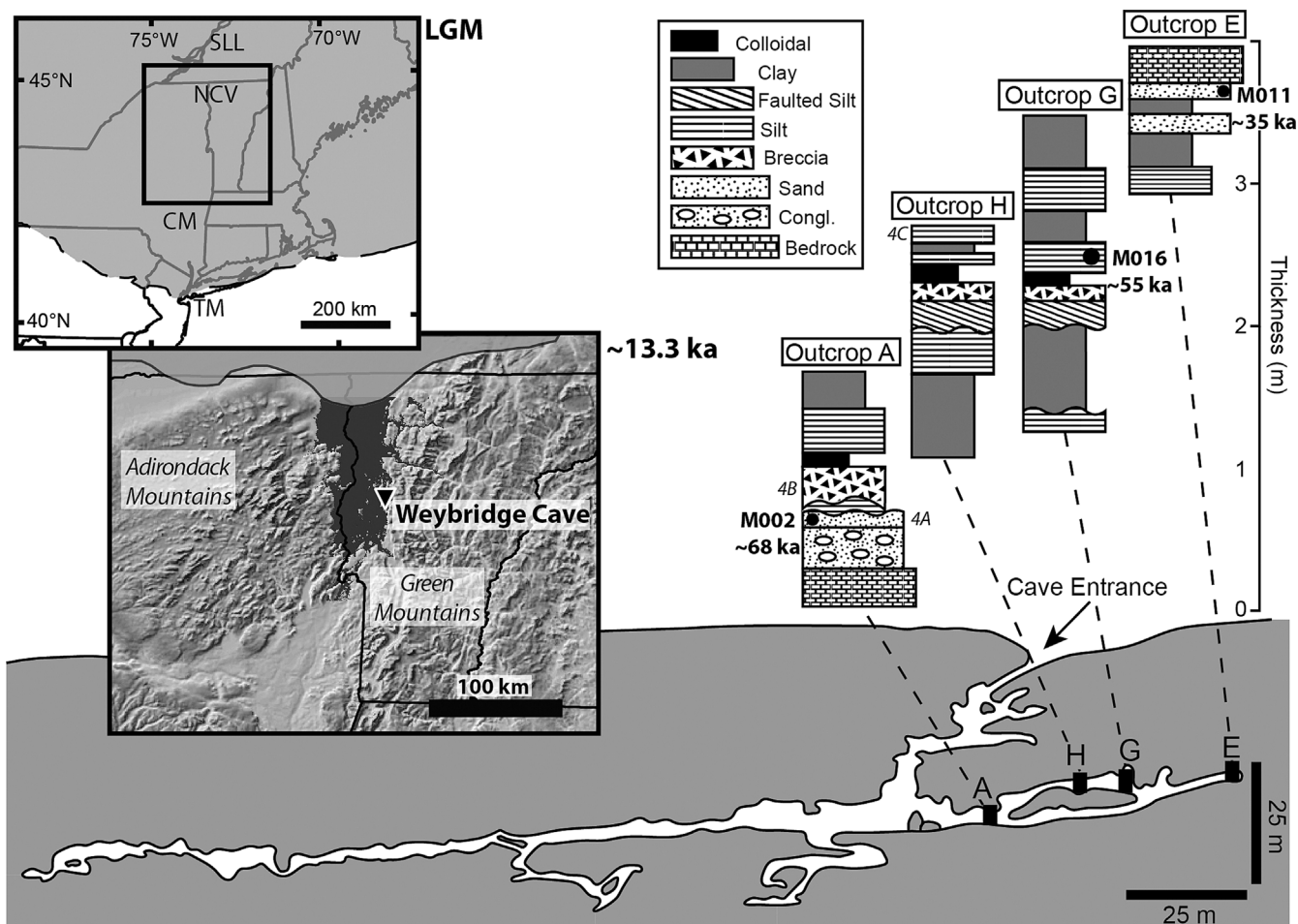
Figure 1. Location of Weybridge Cave, sedimentology and stratigraphy of the studied outcrops (Congl. = Conglomerate), positions and ages of luminescence samples M002, M016 and M011, and locations of photos shown in Fig. 4. Light gray shading on the upper left map (LGM) represents ice extent during the LGM (Dyke et al., 2002). Light gray shading on the inset map (~13.3 ka) represents an approximate ice margin during the Fort Ann stage (dark gray) of proglacial Glacial Lake Vermont (~13.3 ka). Note that Weybridge Cave would be submerged by Glacial Lake Vermont whenever ice advanced south of the St. Lawrence Lowland. SLL, St. Lawrence Lowland; NCV, northern Champlain Valley (sill for flooding the Weybridge Cave region); CM, Catskill Mountains; TM, Terminal Moraine.

Figure 2. Plastic U-channel and prepared face of Outcrop A (visible height, ∼50 cm). Fine laminations are clearly visible, as is a high-angle normal fault offsetting layers on the right side of the cleaned face.

U-channels were scraped to reveal a clean face, described and photographed, and subsamples were taken for grain size analysis using laser scattering with a Horiba LA-950 analyser. Subsamples were also processed to concentrate pollen, but yielded fewer than 50 grains g^{-1}, probably because pollen is susceptible to bacterial degradation in cave environments (Carrión *et al.*, 1999).

Dataloggers for recording temperature, relative humidity and water depth were also deployed at various locations to better understand the cave environment. All were set to record automatically at 1-h intervals.

Luminescence measurements

Sample preparation

A chronology for these sediments was developed using optically stimulated luminescence (OSL) and infrared stimulated luminescence (IRSL) dating (Huntley *et al.*, 1985; Aitken, 1992). All luminescence samples were collected by hammering a 20-cm-long metal tube into the scraped face of an outcrop. Tubes were removed and capped while caving lights were off, eliminating the potential for resetting of the luminescence signal. Tubes were opened in the Middlebury College Luminescence Lab under a dimmed 589-nm sodium lamp fitted with a Lee 101 filter. Following overnight treatments in 10% HCl and bleach, modal size fractions (165–250 μm) of each sample underwent multiple density separations in lithium heteropolytungstate to obtain a quartz fraction (ρ = 2.56–2.70 g mL^{-1}) and a potassium-rich feldspar fraction (ρ < 2.56 g mL^{-1}). Quartz samples then underwent one to three 30-min etches in concentrated HF before a final rinse in concentrated HCl, whereas potassium-rich feldspar

samples were etched for 40 min in 10% HF followed by an HCl rinse. All samples were sieved again following HF etching to ensure measurement of intact, high-quality grains.

Luminescence protocols

Sample analyses were performed on a Daybreak 2200 reader manufactured by Bortolot Daybreak. All samples were analysed using 9.8-mm-diameter aluminum discs with a thickness of 0.5 mm. Photons were recorded using a 9235QA photomultiplier tube manufactured by Electron Tubes with a dark count rate of roughly 20 c.p.s. Stimulation was performed with blue LEDs (480 nm) for quartz and infrared LEDs (880 nm) for feldspar. For quartz analyses measured light was filtered using a Schott UG-11 and Edmunds UG-340 filter pack with an approximate admittance window from 260 to 390 nm, peaked at ∼330 nm. Feldspar analyses were filtered with an Edmunds BG-39 and Kopp 759 filter pack with an admittance window of 320–480 nm, peaked at ∼380 nm.

Irradiations were performed using a 3.7 GBq ^{90}Sr beta source manufactured by Eckert and Ziegler. Source calibration was performed with two different sets of gamma-irradiated calibration quartz: Risø batches 71 and 98. Because batch 71 is not thermally annealed whereas batch 98 is, these two calibration standards yield different sensitivities. Nonetheless, accepting only analyses for which the first and second test dose of a given aliquot agree to within 5% yields tight agreement between the two standards and a nominal dose rate of 0.0618 ± 0.002 Gy s^{-1} on 31 May 2015 (2σ uncertainty).

Samples were analysed using the SAR protocol for quartz (Murray and Wintle, 2000) and the post-infrared infrared (pIRIR) protocol for K-feldspar (Buylaert *et al.*, 2009). Both protocols involved six luminescence measurements: natural, regen-1, regen-2, regen-3, zero dose and regen-1′. Due to the dim nature of the quartz it was not possible to perform a preheat plateau test, so analyses were run at cutheat temperature of 160 °C and preheat temperature of 240 °C. Dose recovery tests on selected bright aliquots of quartz revealed recovery of the administered dose to within 5%. An additional 'IR check' was administered by applying an additional test dose to the aliquot, preheating it, and then measuring the response to infrared stimulation at room temperature.

Experimentation with individual quartz grains from sample M002 demonstrated that only 0.6% (n = 843) of grains gave a measurable response to a 30-Gy test dose, suggesting that signals from larger, multi-grain aliquots are dominated by one or two individual grains. Thus, all remaining quartz samples were analysed using 50–100-grain aliquots. Overall, many of the quartz aliquots analysed displayed very dim luminescence properties, causing a significant number to fail quality assurance tests due to poor counting statistics from weak shine-down curves. Single-grain feldspars were run in the same 'reconnaissance' manner and generally displayed higher luminescence intensities, yielding a higher rate of accepted aliquots.

The pIRIR method used a preheat of 250 °C followed by a low temperature shine-down at 50 °C and a high temperature shine-down at 225 °C. For dose recovery tests, feldspar grains were bleached overnight under a full spectrum floodlight, given a beta dose of 200 Gy, left to rest for 24 h and measured using the full SAR procedure. Dose recovery tests on 23 feldspar grains yielded an average recovery ratio of 0.99 ± 0.02, demonstrating the applicability of the post-IR IRSL protocol for these samples.

IRSL of feldspars has been shown to systematically underestimate the known age of some samples due to anomalous fading of the luminescence signal over time (e.g. Huntley and Lamothe, 2001). Although the post-IR IRSL approach exploits traps that exhibit less fading than conventional IRSL (Buylaert et al., 2009), in some cases this signal still displays non-trivial fading rates (e.g. Thiel et al., 2011; Li et al., 2014). In recognition of this complication, a subset of feldspar grains ($n = 64$) that passed SAR quality assurance statistics (Murray and Wintle, 2000) underwent fading tests. Grains analysed were irradiated, immediately preheated, and then stored for periods of 1, 2, 10 and >250 h before measurement. The spread in measured fading constants was wide (−23 to 13% per decade) and included some negative values. We speculate that the repeated irradiation–preheat–bleach cycling performed in the course of four full SAR analyses [equivalent dose (D_e) estimation, dose recovery test, measurement of the unbleachable component and fading analyses] increased the density of traps causing certain grains to behave differently than they would in nature. Such changes would have a larger effect on grains with initially low luminescence sensitivity than on those that were originally highly sensitive. Fading test results were therefore culled using two criteria: reproducibility of the test dose within 10% and an initial luminescence peak >100 c.p.s. After filtering out these lower quality fading estimates, measured fading rates range from 1 to 8% per decade (mean of $5.05 \pm 0.83\%$ per decade, $n = 14$). This mean fading constant was applied to all PIRIR analyses.

Data reduction

Net luminescence signals were computed by subtracting the measured counts in the first 0.5 s from the measured counts in seconds 20–25 divided by 10. Early background correction was not used for quartz analyses because it degraded precision too severely. Luminescence signals from quartz aliquots showed a weak fast component, with typical fast ratios in the range of 2–10. D_e and associated uncertainties were estimated by fitting a quadratic function to all the data, including the zero dose. For small aliquots an additional uncertainty of 7% was added to reflect intrinsic variability in measured dose rate distributions beyond those already accounted for by counting statistics and curve-fitting (e.g. Medialdea et al., 2014).

Three main quality criteria were used to reject D_e estimates: the recycling test, recuperation test and the test-dose reproducibility ratio (the maximum difference between the first and second test dose). The cutoff for all three tests was 10%. The average recycling ratio and recuperation for the aliquots used were 1.02 ± 0.005 ($n = 165$) and $2.22 \pm 0.23\%$ ($n = 165$), respectively.

Burial doses

Burial doses for all samples were computed using the three-component minimum age model (MAM) (Galbraith et al., 1999). The MAM was considered more appropriate than a central age model because of the likelihood that samples were incompletely bleached during their short transport from the surrounding landscape into the cave. Statistical support for this decision is provided by the positive skewness (0.36–1.29) and high overdispersion (14–76%) of equivalent dose distributions (Galbraith et al., 1999). Furthermore, a small number of K-feldspar aliquots were at or near saturation. This is not surprising given that the pIRIR signal is not easily reset in nature (Buylaert et al., 2009).

Dose rate calculations

Dose rates were calculated through ICP-MS bulk geochemistry of representative sediment collected within a 30-cm radius of each sample (Guérin et al., 2011). Analyses were performed by ALS Minerals in Reno, NV, USA, using a lithium-metaborate fusion. Dose rates were computed using the conversion factors of Guérin et al. (2011), appropriate H_2O attenuation coefficients (Aitken, 1989), and Beta attenuation factors for U, Th and K (Mejdahl, 1979) and Rb (Readhead, 2002). For single grain feldspar samples, internal dose rates were calculated using an average potassium content of 12.23%. This value reflects the mean concentration of a subset ($n = 27$) of accepted feldspar grains that were mounted in epoxy, polished and analysed on a Tescan Vega3 scanning electron microscope equipped with an energy dispersive X-ray spectroscopy detector (SEM-EDS). Direct alpha dose was assumed to be zero given that grains were etched in HF before analysis. Cosmogenic production was also neglected given that samples were shielded by ∼30 m of limestone bedrock. Dose rates calculated by this method were within 2% of values generated by the DRAC calculator (Durcan et al., 2015).

Moisture contents were computed after drying in an oven for 2 days at 65 °C. These values were used to estimate the radiation attenuation due to water, with an estimated 10% variability over the life of the sample. Low uncertainty is justified by the constant relative humidity of 99.9% measured by dataloggers within the cave.

Paleomagnetic measurements

U-channels were analysed for natural and anhysteretic remanent magnetizations (NRM and ARM) on a 2G Enterprises 755 three-axis, pass-through cryogenic magnetometer equipped with a three-axis alternating field (AF) demagnetizer and a 2G 660 Pulse Magnetizer. A single pilot sample was AF demagnetized in 5-mT steps up to a peak field of 100 mT, but detectable residual NRM remained even after the 100-mT step. All other samples underwent a series of 11 AF steps between 5 and 80 mT. ARM was imparted to each sample by applying a 0.1-mT DC field in the presence of a peak AF field of 100 mT. Low-field magnetic susceptibility (χ) for each U-channel was also measured on a Bartington MS2 system. Characteristic remanent magnetization directions for each U-channel were calculated from orthogonal demagnetization plots using PuffinPlot (Lurcock and Wilson, 2012). Data points in Zijderveld plots (Fig. 3) were highly co-linear and principal components computed on the 20–80 mT interval yielded maximum angular deviation values in the range of 2–3°.

Results

Sedimentology and stratigraphy

A composite stratigraphy for the sediments partially infilling the main trunk of Weybridge Cave was constructed from the four studied outcrops (Fig. 1). Outcrop A is the only exposure that reached bedrock where a partially cemented conglomerate of rounded cobbles and pebbles was observed overlying the limestone. Clasts in the conglomerate are predominantly quartzite and were probably washed into the cave from surficial sediments like the erratic-rich till surrounding the entrance today. The conglomerate is overlain at the base of Outcrop A by a layer of coarse sand (Figs 1 and 4A). Sand grains in this unit are rounded and consistently ∼1 mm in diameter, with less frequent coarser sand and granules. Most grains are quartz, with varying degrees of iron staining.
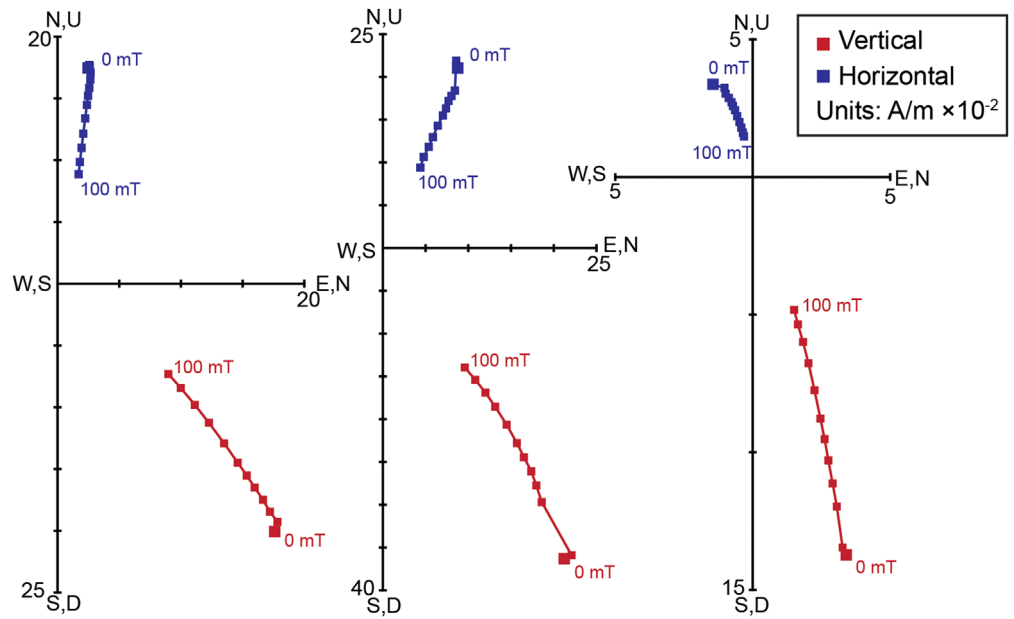
Figure 3. Example Zijderveld plots of the natural remanent magnetization (NRM) for three different locations in Outcrop G. Plots were prepared with Puffin-Plot (Lurcock and Wilson, 2012).
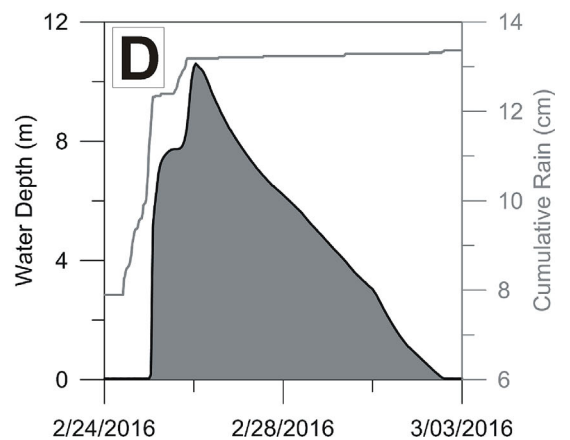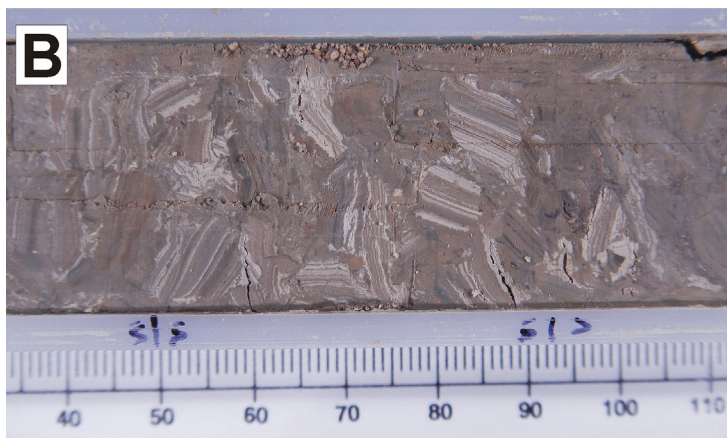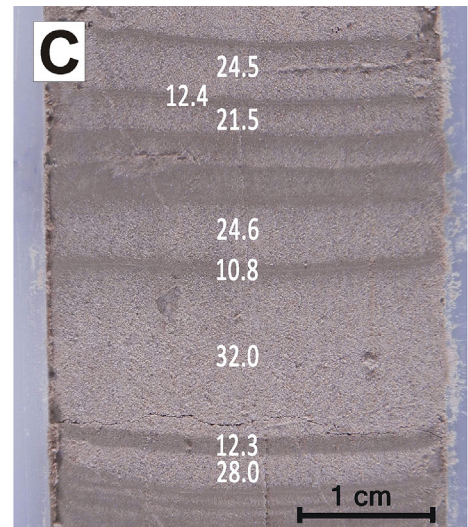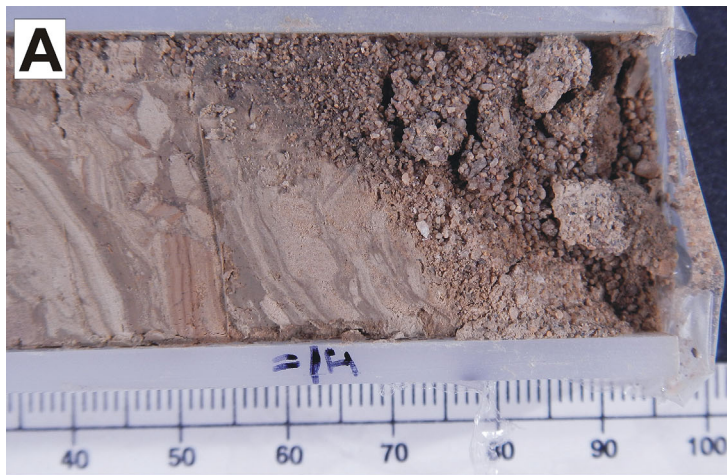
Figure 4. Photographs of clastic sediments sampled in Weybridge Cave. (A) Photo of sand in U-channel (top to the left) from the base of Outcrop A. Scale in centimeters. The basal sand yielded an OSL age of 68.0 ± 10.8 ka. (B) Breccia with intact rip-up clasts of laminated silty clay in U-channel (top to the left) from Outcrop A. Scale in centimeters. This high-energy deposit is capped by a layer of extremely fine sediment (not shown) demonstrating an abrupt change in energy of the depositional environment in the cave. A proposed mechanism is presented in Fig. 7. (C) Close-up of finely laminated sediment in the upper part of Outcrop H (Fig. 1). Values are modal grain sizes in microns determined through laser scattering with a Horiba LA-950 analyser. (D) Water depth in Weybridge Cave (filled, dark gray) and cumulative precipitation measured 5 km away at Middlebury, VT, during a rainstorm in late February 2016 (light gray line). A pulse of heavy rainfall flooded the lower passage of the cave with more than 10 m of standing water that persisted for 6 days.

The sand in Outcrop A is unconformably overlain by ~15 cm of fine silt, with a median grain size of ~8 μm. The silt unit contains two visually distinct end-members: a light gray (10YR 7/1) unit and a gray (10YR 5/1) unit. The bottom 5 cm of the silt features wavy, rhythmic interlaminations of these two colors. Moving upward, the intermixing of these two colors becomes more chaotic, with numerous small-scale angular offsets and broken layers. After 10 cm the silt grades into a visually striking breccia containing rip-up clasts of very dark gray (10YR 3/1), finely laminated silty clay (Figs 1 and 4B). The median grain size of the breccia is coarser (18 μm), with ~60% of the grain size distribution in the coarse and median silt classes. Rip-up clasts are blocky, ~1 cm in size, and are randomly oriented. Laminations within the rip-up clasts are generally <1 mm thick.

The breccia in Outcrop A is capped by 15 cm of very dark gray (10YR 3/1) very fine silt containing reddish brown (5YR 5/3) laminations (≤1 mm thick). The laminations are generally intact, and the unit fines upward to a median grain size of 0.2 μm at the top, with 72% of the grain size distribution <2 μm.

The fine layer capping the breccia in Outcrop A grades upward conformably into horizontally laminated very fine silty clay with a median grain size of ~5 μm. The modal grain size in this unit is very fine silt (~50%), identical to the chaotic silt underlying the breccia. Layers range from 1 to 10 mm in thickness and are visible as alternations between light gray (10YR 7/1) and dark gray (10YR 4/1) colors. On the basis of appearance and grain size distribution, this unit is correlated to the laminated very fine silt at the base of Outcrops G and H (Figs 1 and 4C), both of which contain a second breccia overlain by colloidal sediment (Fig. 1). Median grain sizes decreases upward through Outcrops G and H, reaching minima of <4 μm near the top. The matrix of the breccia in each has a median size (6–10 μm) roughly double that of the rip-up clasts within it (3–6 μm).

Silty clay in the upper part of Outcrop G is correlated to a similar unit at the base of Outcrop E (Fig. 1), which is capped by a layer of medium, laminated sand that reaches the cave ceiling.

Geochronology

Luminescence ages were generated for three samples collected from coarser sections of the stratigraphy (Figs 1 and 5). Sample M002 was collected from the sand overlying the conglomerate at the base of Outcrop A (Fig. 1). Analysis using the quartz OSL technique yielded an age of 68.0 ± 10.8 ka (Fig. 5; Table 1).
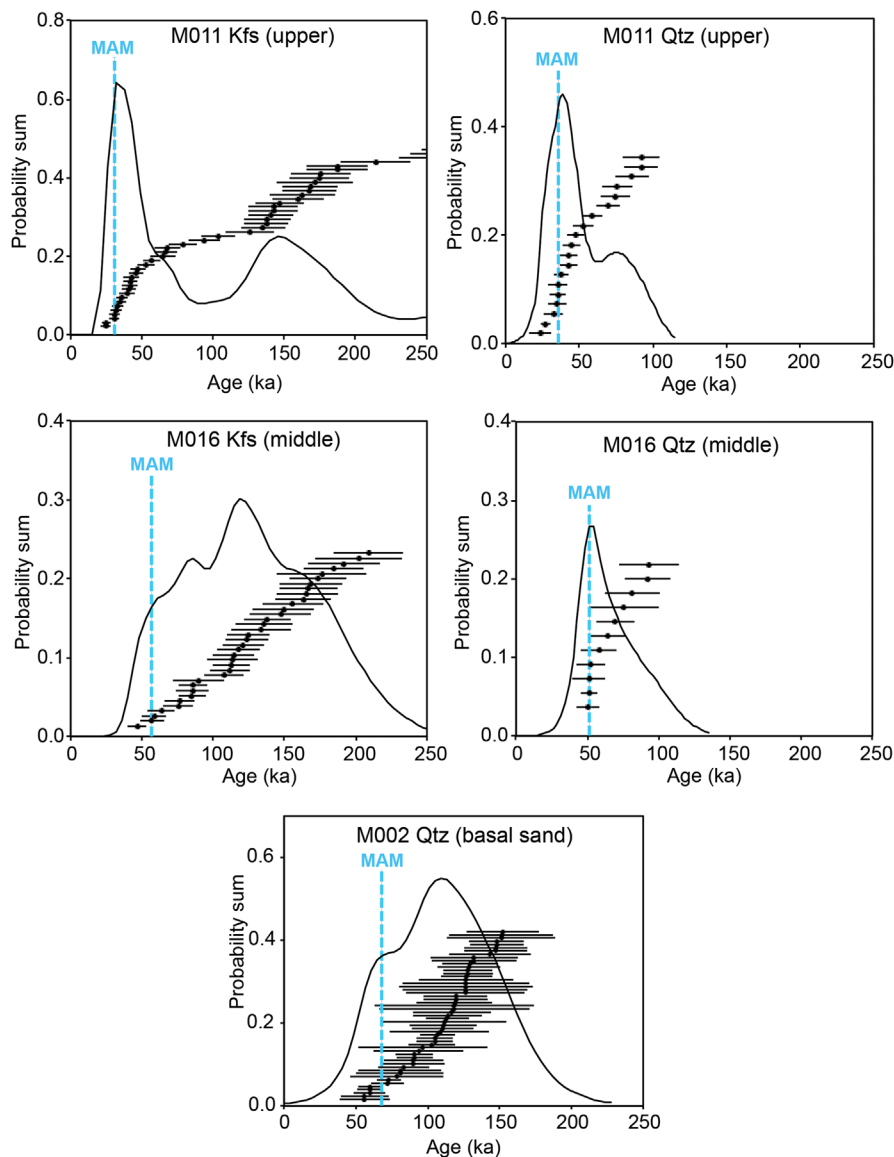
Figure 5. Probability density functions for feldspar IRSL and quartz OSL age estimates. The dashed blue lines show minimum age model (MAM) estimates. Ages and error bars are shown with 2-sigma uncertainty.

Table 1. Small-aliquot quartz OSL results.

Sample	n	K (%)	Th (ppm)	U (ppm)	Rb (ppm)	Water (%)	Dose rate (Gy ka^{-1})	Overdispersion (%)	Age model	Age (ka)
M011	19	2.63 ± 0.01	5.9 ± 0.2	1.1 ± 0.1	72.8 ± 0.1	9.8	2.96 ± 0.20	36 ± 7	MAM	36.1 ± 6.6
M016	12	2.75 ± 0.01	5.3 ± 0.2	1.2 ± 0.1	67.8 ± 0.1	16.5	2.84 ± 0.22	14 ± 8	MAM	51.8 ± 14.7
M002	53	1.81 ± 0.01	4.8 ± 0.2	1.1 ± 0.1	61.7 ± 0.1	17.9	1.99 ± 0.16	21 ± 4	MAM	68.0 ± 10.8

This result indicates that sediment at the base of Outcrop A was deposited during MIS-4. Sample M016 was collected from a slightly coarser layer near the stratigraphic center of Outcrop G (Fig. 1). Quartz OSL yielded an age of 51.8 ± 14.7 ka (Fig. 5; Table 1), and IRSL on feldspar yielded an overlapping age of 56.7 ± 16.0 ka (Fig. 5; Table 2). Thus, sediment near the center of Outcrop G was most likely deposited during the early part of MIS-3. Finally, sample M011 was collected from the coarse sand capping Outcrop E (Fig. 1). This sample generated a quartz OSL age of 36.1 ± 6.6 ka (Fig. 5; Table 1) and an overlapping feldspar IRSL age of 32.5 ± 5.7 ka (Fig. 5; Table 2) indicating deposition during MIS-2.

Paleomagnetism

Paleomagnetic intensity measurements from the sections were visually correlated to the Global Paleointensity Stack since 75 ka, the GLOPIS-75 (Laj et al., 2004). The Weybridge Cave sediments are considered appropriate for magnetic paleointensity studies because the concentration-dependent parameters ARM and χ vary by less than a factor of 4 and plots of the grain-size-dependent ratio ARM/χ show minimal scatter, indicating that variations in concentration and grain size are inconsequential. Furthermore, normalizing NRM intensity by either ARM or χ produces similar paleointensity curves (Tauxe, 1993). The most distinct feature in the GLOPIS-75 record (Laj et al., 2004) is the Laschamp excursion, a sharp drop in paleointensity at 41.10 ± 0.35 ka (Lascu et al., 2016). The paleomagnetic record from outcrop G exhibits a similar paleointensity low accompanied by a large ($>35°$) change in inclination and a local maximum in declination (Fig. 6). Applying a linear stretch to the Weybridge Cave paleomagnetic record using the Laschamp excursion and the quartz OSL age from outcrop G (Fig. 1) as tie points reveals a strong visual correlation between the two curves during the period from $\sim$35 to 55 ka (Fig. 6).

Discussion

Sedimentary environment

To interpret the clastic sedimentary package within Weybridge Cave it is necessary to first determine the most likely mechanism for its deposition. The basal gravel containing rounded allochthonous clasts in excess of 10 cm in diameter clearly reflects an inflowing stream of high competence. The lowest accessible part of the cave is currently blocked by a leaking plug of sediment; drainage must have been less restricted during deposition of the sandy gravel, allowing a greater through-flowing discharge capable of transporting these clasts. The OSL age of $\sim$68 ka from the sand overlying

the basal gravel is consistent with through-flowing conditions during MIS-4, but the history of the cave proceeding that time is impossible to determine.

The finer sediments comprising the bulk of the four exposures are interpreted to have been deposited when the surrounding landscape was subaerial but the cave was partially filled with standing water. The thin horizontal laminations, micro-scale graded bedding, and parallel sedimentary contacts (Fig. 4C), combined with the fine grain size of the sediment and lack of ripples or cross-bedding, indicate deposition by suspension settling from still water. Identical sediments have been reported from other caves and attributed to events at the surface that delivered pulses of sediment to a partially water-filled cave environment (Bull, 1981; Gillieson, 1986). Direct observations and data from temperature and water-level loggers reveal that the lower parts of Weybridge Cave fill with standing water during intense rain or snowmelt events today (Fig. 4D). It is reasonable to assume that similar conditions existed in the past, and blocking of the lower parts of the cave system by leaking plugs of sediment could explain the switch from high-energy, through-flowing conditions recorded by the basal conglomerate and coarse sand at Outcrop A.

Other possible depositional environments for the fine laminated sediments are less compatible with the properties and physical location of these deposits. For instance, some-what similar sediments have been reported from water-filled subglacial caves (Larsen et al., 1987; Valen et al., 1997; Ward et al., 2003; Weremeichik and Mylroie, 2014) but in all of these examples the point of deposition was close to the cave entrance. In the case of Weybridge Cave it is unlikely that the sediment comprising these deposits could be transported deep into the intricate network of passageways in the absence of through-flowing conditions. Fine, laminated cave sediments have also been interpreted as proglacial lake deposits (Wood et al., 2010). However, in contrast with Weybridge Cave these deposits feature ripples and other sedimentary evidence for flowing water (Wood et al., 2010). They are also restricted to positions near large cave entrances, unlike those in Weybridge Cave that are found deep underground in narrow passageways.

Finally, the breccia units overlain by extremely fine sediment observed in Outcrops A, G and H (Fig. 1) indicate a dramatic shift from a high-energy erosional regime to a very low-energy depositional environment. Specifically, the breccia layers contain obvious rip-up clasts of laminated silt (Fig. 4B), requiring that sediments elsewhere in the cave were eroding when these units were deposited. In contrast, the capping clay layer contains over 70% material $<2\,\mu m$ in diameter, suggesting deposition under extremely still conditions. We propose that these layers formed when a sediment

Table 2. Single-grain feldspar IRSL results.

Sample	n	K (%)	Th (ppm)	U (ppm)	Rb (ppm)	Water (%)	Dose rate (Gy ka^{-1})	Overdispersion (%)	Uncorrected age (ka)	Fading-corrected age (ka)
M011	46	2.63 ± 0.01	5.9 ± 0.2	1.1 ± 0.1	72.8 ± 0.1	9.8	4.09 ± 0.28	76 ± 8	22.1 ± 3.2	32.5 ± 5.7
M016	35	2.75 ± 0.01	5.3 ± 0.2	1.2 ± 0.1	67.8 ± 0.1	16.5	3.97 ± 0.30	36 ± 5	38.0 ± 10.7	56.7 ± 16.0
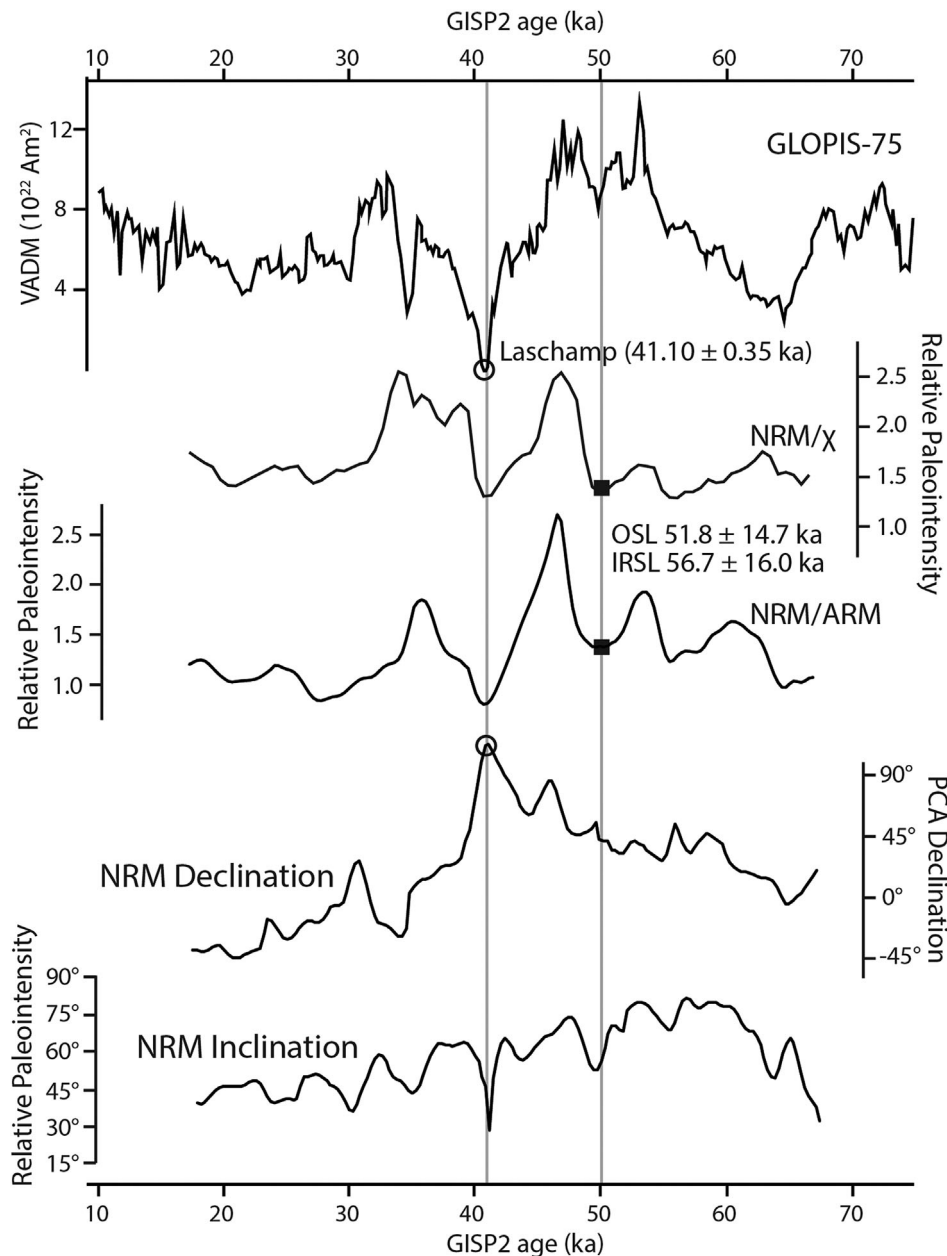
Figure 6. Relative paleointensity curves for Weybridge Cave correlated to the GLOPIS-75 record (Laj *et al.*, 2004) using the Laschamp excursion and the quartz OSL age from Outcrop G as tie points (grey lines). Natural and anhysteretic remanent magnetization (NRM/ARM) intensities were calculated following the 20-mT demagnetization step. Note that linear stretching of the Weybridge Cave record beyond the tie points yields an apparent correlation that extends to an unrealistically young age (<20 ka) given the luminescence ages of ~35 ka for Outcrop E. However, the stratigraphy observed in the outcrops suggests strongly that the sedimentation rate varied over time making linear extrapolation away from the tie points increasingly tenuous. Thus, the younger parts of the Outcrop G paleointensity record cannot be directly correlated to GLOPIS-75 in the absence of additional age control.

plug impounding water within the cave abruptly failed, leading to a rapid drainage event that eroded and redistributed sediment within the cave system. Subsequent re-plugging of the outlet by sedimentation or mass wasting terminated the high-energy drainage, quickly reverting to slackwater conditions from which the overlying clay-rich units could settle (Fig. 7). The presence of (at least) two separate breccia units in the composite stratigraphy indicates that this sequence of events occurred multiple times. Such dramatic fluctuations are incompatible with submergence of the cave beneath a proglacial lake or ice sheet where hydraulic head would be invariant over the length of the cave system. Overall, transport of clastic sediment into Weybridge Cave from a subaerial landscape is the interpretation most consistent with available evidence.

Implications

Because the location of Weybridge Cave would be inundated by proglacial lake water when the LIS blocks the valley farther north (Chapman, 1937), as was the case for Glacial Lake Vermont (Fig. 1), subaerial conditions at the cave

entrance require that the ice margin is north of the SLL. Thus, the basal age of ~68 ka, the age of ~55 ka from Outcrop G and the age of ~35 ka for the capping sand at Outcrop E (Fig. 1) all represent times when the southern margin of the LIS was north of the SLL. Due to the discontinuous nature of the stratigraphic record in the cave it is not possible to rule out whether the Champlain Valley was occupied by a short-lived proglacial lake or ice advance during the Early Wisconsinan (MIS-4). Some numerical modeling experiments (Stokes *et al.*, 2012) and dates from some pre-Late Wisconsinan tills (Lamothe *et al.*, 1992; Colgan and Newman, 1999) suggest that ice advanced into this region during MIS-4. Either way it is clear that the southern margin of the LIS was north of the SLL at ~35 ka, which is consistent with numerical modeling results (Stokes *et al.*, 2012).

By combining the youngest OSL age with constraints from other studies it is possible to elucidate the history of LIS advance through the north-eastern USA leading up to the MIS-2 glacial maximum. Radiocarbon ages of 33 250 ± 240 [14]C a BP for terrestrial plant remains in alluvial sands from the SLL calibrate to ~37.5 ka BP (Parent *et al.*, 2015). These sands are capped by a layer of fossiliferous sediment
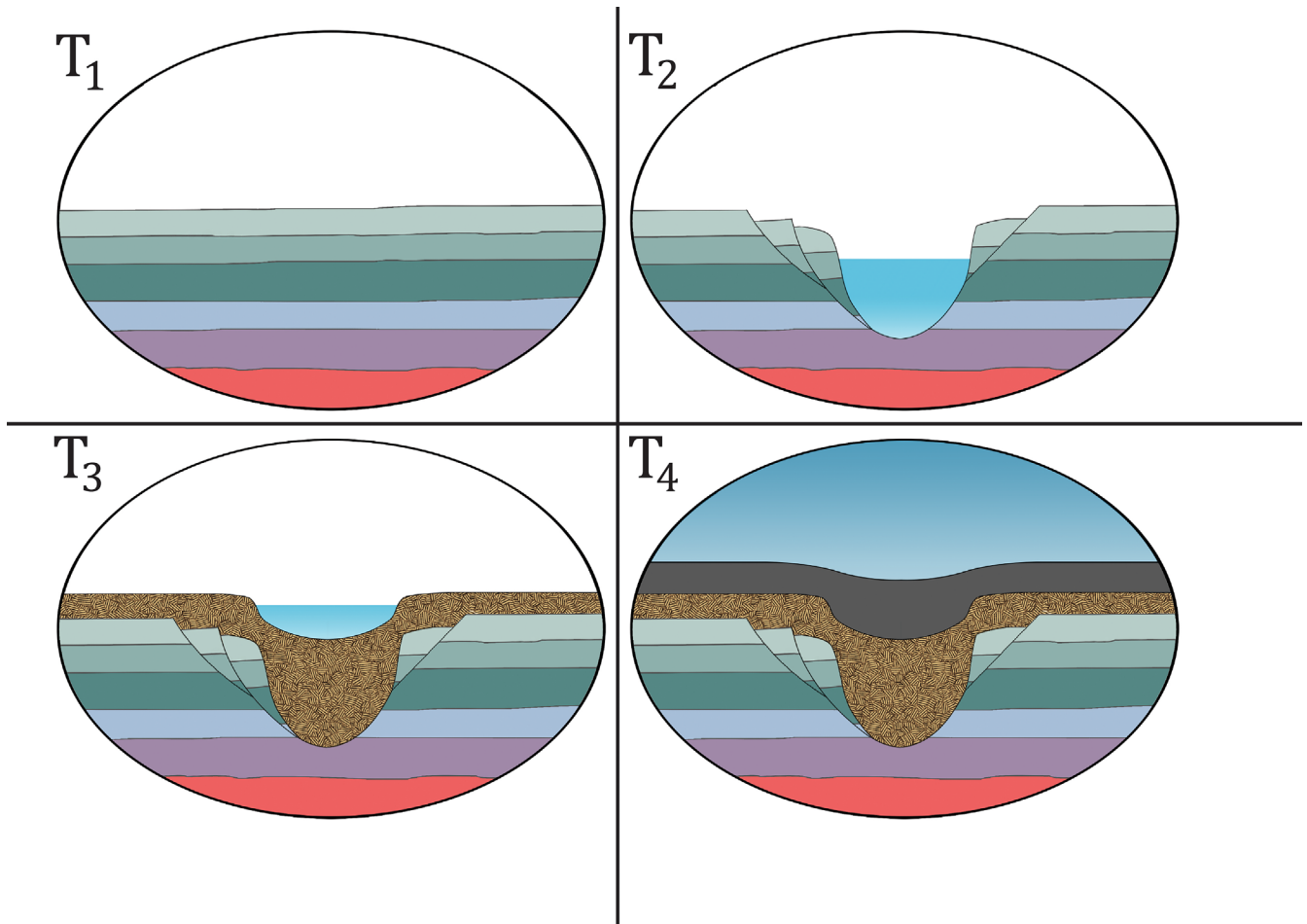
Figure 7. Cartoon showing a proposed mechanism for deposition of the breccia layers with capping fines. First, failure of a sediment plug blocking drainage deeper in the cave led to a sudden increase in through-flowing water that incised finely laminated deposits (T_1), causing slumping of adjacent strata (T_2). As upstream outcrops were eroded and the system aggraded, sediments were buried beneath a breccia of rip-up clasts (T_3). Excessive sediment load plugged the cave outflow, causing standing water within the cave and deposition of a capping layer of very fine-grained sediment (T_4).

representing a marine incursion into the SLL, requiring that the LIS was north of the SLL at that time (Fig. 8A). The luminescence ages of ~35 ka from the top of Outcrop E indicate that Weybridge Cave was not yet inundated by a proglacial lake. Thus, the southern margin of the LIS did not advance into the northern Champlain Valley until after 35 ka (Fig. 8B). In contrast, Laurentide ice had reached the Catskill Mountains in southern New York by ~28 ka (Fig. 8C) as demonstrated by an OSL age of 27 580 ± 740 a on glaciola-custrine sediments preserved beneath LGM till (Rayburn, 2015). Relatively thick ice in the Hudson Valley is necessary to impound water in this ice-marginal basin, so the actual southern margin of the ice sheet may have been south of this position at this time. Nonetheless this age constrains arrival of the LIS at this latitude. Radiocarbon ages from the terminal moraine on Long Island, New York, suggest that the LIS reached its maximum extent by 21 750 ± 750 ^{14}C a BP (~26 cal ka BP), if not earlier (Dyke et al., 2002; Mickelson and Colgan, 2003; Ridge, 2004). This estimate is supported by cosmogenic surface-exposure dates for erratic boulders on the terminal moraine (Balco et al., 2002; Balco and Schaefer, 2006).

Plotting of these data on a time–distance diagram (Fig. 9) reveals an overall average ice advance rate of ~50 m a^{-1} over a distance >600 km. However, it is important to note that the two northernmost ages are maximum limiting: the SLL was ice free until after 37.5 ka (Parent et al., 2015), and the LIS had not yet advanced into the northern Champlain

Valley (NCV), which would inundate Weybridge Cave beneath a proglacial lake, at 35 ka. Similarly, the age of 26 ka for the terminal moraine is minimum limiting because it is not known exactly when the ice sheet margin reached this position. In contrast, the age from the small ice-marginal lake in the Catskills is more direct, indicating that the LIS blocked the east-flowing drainage at that time (Rayburn, 2015). Nonetheless, estimates of advance rates derived from these ages are revealing to a first order, and comparisons between these rates remain useful for illuminating ice-margin behavior.

Taking these age limits at face value the point-to-point advance rate was slowest (25 m a^{-1}) between the SLL and the NCV. Although the robustness of this estimate is low because the ages are minimum limiting, a slow rate is consistent with ice advance up the adverse slope from the SLL into the Champlain Valley. Given that the LIS advanced ~400 km from the NCV to the Catskill Mountains in less than 7000 a, the rate appears to have roughly doubled as the terminus advanced down the Champlain Valley. Because a proglacial lake presumably filled the north-draining valley in front of the advancing ice margin (Fig. 8B), as Glacial Lake Vermont did during retreat (Chapman, 1937), accelerated ice advance may have been facilitated by subglacial deformation of fine-grained water-saturated sediment (van der Meer et al., 2003) or ice streaming as has been documented during ice retreat (Wright, 2015). Uncertainty over when the ice reached the terminal moraine position complicates calculation of an
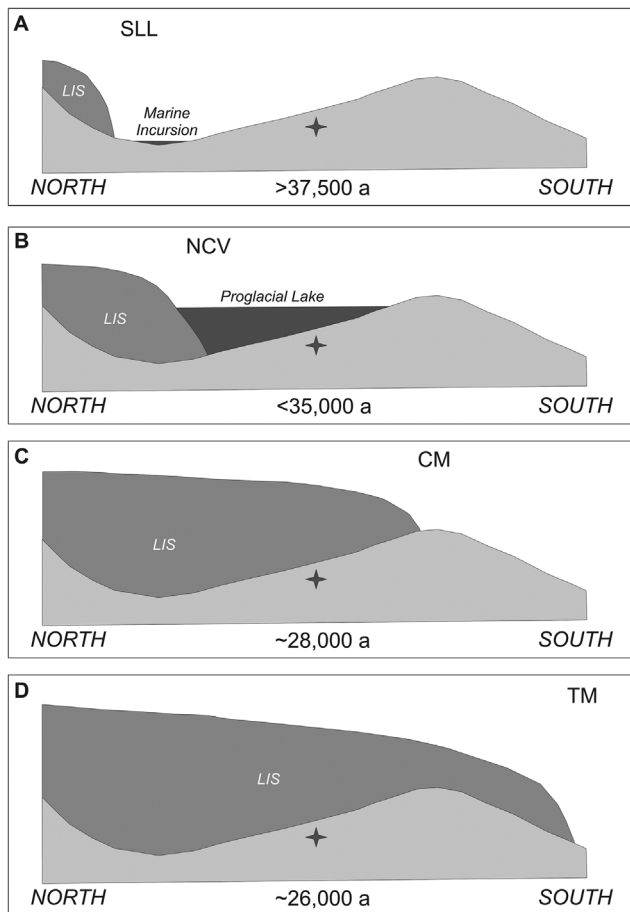
Figure 8. Schematic north–south transect illustrating constraints on the southern border of the Laurentide Ice Sheet (LIS) during the lead up to MIS-2. The star marks the location of Weybridge Cave. (A) Calibrated radiocarbon ages on terrestrial macrofossils from the St. Lawrence Lowland (SLL) indicate ice-free conditions followed by a marine incursion *ca.* 37.5 ka BP (Parent *et al.*, 2015). (B) Luminescence ages from Weybridge Cave indicate that the LIS advanced into the northern Champlain Valley (NCV) after 35 ka. (C) The advancing LIS reached the Catskill Mountains (CM) and impounded an ice-marginal lake around 28 ka (Rayburn, 2015). Radiocarbon and cosmogenic surface-exposure ages indicate the LIS had reached its terminal moraine position (TM) by ~26 ka (Dyke *et al.*, 2002; Mickelson and Colgan, 2003; Ridge, 2004).

Figure 9. OSL ages (purple circles) and IRSL ages (purple triangles) from Weybridge Cave (offset for clarity and presented with 1-sigma errors) compared with the marine $\delta^{18}O$ record (‰, note reversed scale, Lisiecki and Raymo, 2005) and a global sea-level (GSL) reconstruction (Lambeck *et al.*, 2014). Marine Oxygen Isotope Stages 1–5a are shown (Lisiecki and Raymo, 2005), along with classical divisions of the Laurentide glacial record: H, Holocene; LW, Late Wisconsinan; MW, Middle Wisconsinan; EW, Early Wisconsinan. Top shows time–distance relationships for the advancing Laurentide Ice Sheet, with advance rates in $m\,a^{-1}$. SLL, St. Lawrence Lowland (Parent *et al.*, 2015); NCV, northern Champlain Valley [sill for flooding the Weybridge Cave (WC) region]; CM, Catskill Mountains (Rayburn, 2015); TM, Terminal Moraine (Dyke *et al.*, 2002; Mickelson and Colgan, 2003; Ridge, 2004). The dashed red line represents a theoretical maximum advance rate ($150\,m\,a^{-1}$) calculated from an age of 27 ka for LIS arrival at the terminal moraine position, and 28 ka for arrival at the CM.

advance rate through southernmost New York, but the calibrated radiocarbon age of 26 ka yields an advance rate of $\sim100\,m\,a^{-1}$ over the last ~150 km. This rapid advance rate may reflect increasingly positive glacial mass balance as climatic conditions approached the LGM. For comparison, ice retreat rates in the early part of the deglaciation calculated from varve records in the Connecticut River Valley were $50–100\,m\,a^{-1}$, and accelerated to $\sim300\,m\,a^{-1}$ between 14.5 and 14.0 ka (Ridge *et al.*, 2012).

Finally, to consider an end-member scenario, an advance rate of $150\,m\,a^{-1}$ can be calculated assuming an age of 27 ka for arrival of the LIS at its terminal moraine position, and an age of 28 ka for arrival at the Catskill Mountains. Extrapolating this rate back in time yields an estimate of ~31 ka for advance of the LIS across the SLL (Fig. 9). This date is consistent with the minimum limiting nature of the SLL (~37.5 ka) and NCV (~35 ka) ages, although it is unlikely that the LIS advanced at a constant rate over a distance of >600 km. In addition, although reconstructions reveal that global sea level (Fig. 9) dropped rapidly ~31 ka (Lambeck *et al.*, 2014), marine $\delta^{18}O$ began increasing steadily ~50 ka (Lisiecki and Raymo, 2005). This inconsistency undermines efforts to interpret a uniquely Laurentide signal from records

of global ice volume. Furthermore, multi-isotope cosmogenic surface-exposure dating suggests that higher summits in New England were ice covered after ~40 ka (Bierman *et al.*, 2015). Even if this ice took the form of local ice caps, it is unclear why advance of the LIS across the SLL would have lagged the onset of alpine glaciation by 10 ka.

Conclusions

This is the first study to use cave sediment records to constrain past behavior of the LIS in north-eastern North America. Clastic sediments partially infilling the lowest accessible level of Weybridge Cave in the Champlain Valley of western Vermont pre-date the MIS-2 advance of the LIS. A basal sandy conglomerate, deposited before ~68 ka, represents high-energy through-flowing conditions. In contrast, finer sediments overlying this basal unit were deposited when the cave was partially filled with water and the surrounding landscape was subaerial. Direct observations and dataloggers indicate that such conditions are met today at times of intense rainfall or snowmelt events. Sedimentary features including thin horizontal laminations, micro-scale graded bedding and parallel sedimentary contacts, combined with the fine grain size of the sediment and lack of ripples or cross-bedding, indicate deposition from still water. Breccia layers within this stratigraphy were produced when the sedimentary plug blocking drainage from the cave failed, leading to a brief high-energy, erosive event. Layers of extremely fine material capping the breccia units were deposited under standing water conditions after the sedimentary plug was re-established.

The site of Weybridge Cave was inundated by a proglacial lake whenever the LIS advanced south of the SLL in southern Québec. Luminescence ages of ~68, ~55 and ~35 ka from the cave therefore represent times when the LIS was north of the SLL. By combining the youngest of these ages with other chronologic evidence limiting the position of the southern border of the LIS, it is possible to calculate advance rates for the LIS over the 12 ka leading up to the LGM. Rates were relatively slow as the ice ascended the adverse slope out of the SLL, doubled as the margin traversed the Champlain Valley, perhaps aided by subglacial bed deformation, and were fastest (~100 m a^{-1}) as the margin approached the terminal moraine position. These advance rates should be useful to test and refine reconstructions of LIS dynamics leading up to the LGM.

Abbreviations. AF, alternating field; ARM, anyhysteretic remanent magnetization; IRSL, infrared stimulated luminescence; LGM, Last Glacial Maximum; LIS, Laurentide Ice Sheet; MAM, minimum age model; MIS, Marine Isotope Stage; NCV, northern Champlain Valley; NRM, natural remanent magnetization; OSL, optically stimulated luminescence; PIRIR, post-infrared infrared; SLL, St. Lawrence Lowland.

References

Aitken MJ. 1989. Luminescence dating: a guide for non-specialists. *Archaeometry* **31**: 147–159.

Aitken MJ. 1992. Optical dating. *Quaternary Science Reviews* **11**: 127–131.

Balco G, Schaefer J. 2006. Cosmogenic-nuclide and varve chronologies for the deglaciation of southern New England; terrestrial cosmogenic nuclides. *Quaternary Geochronology* **1**: 15–28.

Balco G, Stone JOH, Porter SC et al. 2002. Cosmogenic-nuclide ages for New England coastal moraines, Martha's Vineyard and Cape Cod, Massachusetts, USA. *Quaternary Science Reviews* **21**: 2127–2135.

Berger GW, Eyles N. 1994. Thermoluminescence chronology of Toronto-area Quaternary sediments and implications for the extent of the midcontinent ice sheet (s). *Geology* **22**: 31–34.

Bierman PR, Davis PT, Corbett LB et al. 2015. Cold-based Laurentide ice covered New England's highest summits during the Last Glacial Maximum. *Geology* **43**: 1059–1062.

Bull PA. 1981. Some fine-grained sedimentation phenomena in caves. *Earth Surface Processes and Landforms* **6**: 11–22.

Buylaert JP, Murray AS, Thomsen KJ et al. 2009. Testing the potential of an elevated temperature IRSL signal from K-feldspar. *Radiation Measurements* **44**: 560–565.

Carlson AE, LeGrande AN, Oppo DW et al. 2008. Rapid early Holocene deglaciation of the Laurentide Ice Sheet. *Nature Geoscience* **1**: 620–624.

Carrión JS, Munuera M, Navarro C et al. 1999. The palaeoecoloical potential of pollen records in caves: the case of Mediterranean Spain. *Quaternary Science Reviews* **18**: 1061–1073.

Chapman DH. 1937. Late-glacial and postglacial history of the Champlain Valley. *American Journal of Science* **34**: 89–124.

Clark PU, Dyke AS, Shakun JD, et al. 2009. The last glacial maximum. *Science* **325**: 710–714.

Colgan PM, Newman WA. 1999. Amino acid evidence for the age of the lower till in Boston Harbor, Massachusetts. *Abstracts with Programs – Geological Society of America* **31**: 10.

Durcan JA, King GE, Duller GAT. 2015. DRAC: Dose Rate and Age Calculator for trapped charge dating. *Quaternary Geochronology* **28**: 54–61.

Dyke AS, Andrews JT, Clark PU et al. 2002. The Laurentide and Innuitian ice sheets during the Last Glacial Maximum. *Quaternary Science Reviews* **21**: 9–31.

Fowler BK. 1979. Glacial till on Mount Washington. *Mount Washington Observatory News Bulletin* **20**: 2–4.

Fowler BK. 1999. Pre-late Wisconsinan age for part of the glaciolacustrine stratigraphy, lower Peabody Valley, northern White Mountains, Gorham, New Hampshire; Late Quaternary history of the White Mountains, New Hampshire and adjacent southeastern Québec. *Geographie Physique et Quaternaire* **53**: 109–116.

Galbraith RF, Roberts RG, Laslett GM et al. 1999. Optical dating of single and multiple grains of quartz from jinmium rock shelter, northern Australia: Part i, Experimental design and statistical models. *Archaeometry* **41**: 339–364.

Gibbons AB, Megeath JD, Pierce KL. 1984. Probability of moraine survival in a succession of glacial advances. *Geology* **12**: 327–330.

Gillieson D. 1986. Cave sedimentation in the New Guinea Highlands. *Earth Surface Processes and Landforms* **11**: 533–543.

Goldthwait RP. 1939. Mount Washington in the Great Ice Age. *New England Naturalist* **5**: 12–19.

Guérin G, Mercier N, Adamiec G. 2011. Dose-rate conversion factors: update. *Ancient TL* **29**: 5–8.

Huntley DJ, Godfrey-Smith DI, Thewalt MLW. 1985. Optical dating of sediments. *Nature* **313**: 105–107.

Huntley DJ, Lamothe M. 2001. Ubiquity of anomalous fading in K-feldspars and the measurement and correction for it in optical dating. *Canadian Journal of Earth Sciences* **38**: 1093–1106.

Koteff C, Pessl F. 1985. Till stratigraphy in New Hampshire: correlations with adjacent New England and Québec. *Geological Society of America Special Papers* **197**: 1–12.

Laj C, Kissel C, Beer J. 2004. High resolution global paleointensity stack since 75 kyr (GLOPIS-75) calibrated to absolute values. In *Timescales of the Paleomagnetic Field*, Channell J, Vent D, Lowrie W, Meert J. (eds). Geophysical Monograph Series **145**: 255–265.

Lambeck K, Rouby H, Purcell A, et al. 2014. Sea level and global ice volumes from the Last Glacial Maximum to the Holocene. *Proceedings of the National Academy of Sciences of the United States of America* **111**: 15296–15303.

Lamothe M, Parent M, Shilts WW. 1992. Sangamonian and Early Wisconsinan events in the St. Lawrence Lowland and Appalachians of southern Québec, Canada. *Geological Society of America Special Papers* **270**: 171–184.

Larsen E, Gulliksen S, Lauritzen S et al. 1987. Cave stratigraphy in western Norway; multiple Weichselian glaciations and interstadial vertebrate fauna. *Boreas* **16**: 267–292.

Lascu I, Feinberg JM, Dorale JA et al. 2016. Age of the Laschamp excursion determined by U−Th dating of a speleothem geomagnetic record from North America. *Geology* **44**: 139–142.

Li B, Jacobs Z, Roberts R et al. 2014. Review and assessment of the potential of post-IR IRSL dating methods to circumvent the problem of anomalous fading in feldspar luminescence. *Geochronometria* **41**: 178–201.

Lisiecki LE, Raymo ME. 2005. A Pliocene-Pleistocene stack of 57 globally distributed benthic δ^{18}O records. *Paleoceanography* **20**.

Lowell TV, Fisher TG, Hajdas I et al. 2009. Radiocarbon deglaciation chronology of the Thunder Bay, Ontario area and implications for ice sheet retreat patterns. *Quaternary Science Reviews* **28**: 1597–1607.

Lowell TV, Hayward RK, Denton GH. 1999. Role of climate oscillations in determining ice-margin position: hypothesis, examples, and implications. *Special Papers-Geological Society Of America* **337**: 193–203.

Lurcock PC, Wilson GS. 2012. PuffinPlot: a versatile, user-friendly program for paleomagnetic analysis. *Geochemistry, Geophysics, Geosystems* **13**.

Medialdea A, Thomsen KJ, Murray AS et al. 2014. Reliability of equivalent-dose determination and age-models in the OSL dating of historical and modern palaeoflood sediments. *Quaternary Geochronology* **22**: 11–24.

Mejdahl V. 1979. Thermoluminescence dating: beta-dose attenuation in quartz grains. *Archaeometry* **21**: 61–72.

Mickelson DM, Colgan PM. 2003. The southern Laurentide Ice Sheet. *Developments in Quaternary Sciences* **1**: 1–16.

Muller EH, Sirkin L, Craft JL. 1993. Stratigraphic evidence of a pre-Wisconsinan interglaciation in the Adirondack Mountains, New York. *Quaternary Research* **40**: 163–168.

Murray AS, Wintle AG. 2000. Luminescence dating of quartz using an improved single-aliquot regenerative-dose protocol. *Radiation Measurements* **32**: 57–73.

Oldale R, Colman S. 1992. On the age of the penultimate full glaciation of New England. *Geological Society of America Special Papers* **270**: 163–170.

Palmer AN. 1991. Origin and morphology of limestone caves. *Geological Society of America Bulletin* **103**: 1–21.

Parent M, Lefebvre R, Rivard C *et al.* 2015. Mid-Wisconsinan fluvial and marine sediments in the central St-Lawrence Lowlands; implications for glacial and deglacial events in the Appalachian Uplands. *Abstracts with Programs – Geological Society of America* **47**: 82.

Quick PG, Porter C. 2010. *Vermont Caves: a Geologic and Historical Guide*. Huntsville, AL: National Speleological Society.

Rayburn J. 2015. Age of an ice-dammed lake on the lee side of the Catskill Mountains, New York, and rough estimates for the rate of ice advance to the Last Glacial Maximum. *Geological Society of America, Abstracts with Programs* **47**: 713.

Rayburn JA, Franzi DA, Knuepfer PLK. 2007. Evidence from the Lake Champlain Valley for a later onset of the Champlain Sea and implications for late glacial meltwater routing to the North Atlantic. *Palaeogeography Palaeoclimatology Palaeoecology* **246**: 62–74.

Rayburn JA, Knuepfer PL, Franzi DA. 2005. A series of large, Late Wisconsinan meltwater floods through the Champlain and Hudson valleys, New York State, USA; reassessing the role of meltwater processes during Quaternary glaciations. *Quaternary Science Reviews* **24**: 2410–2419.

Readhead M. 2002. Absorbed dose fraction for ^{87}Rb β particles. *Ancient TL* **20**: 25–28.

Ridge JC. 2004. The Quaternary glaciation of western New England with correlations to surrounding areas. *Developments in Quaternary Sciences* **2**: 169–199.

Ridge JC, Balco G, Bayless RL *et al.* 2012. The new North American varve chronology: a precise record of southeastern Laurentide Ice Sheet deglaciation and climate, 18.2–12.5 kyr BP, and correlations with Greenland ice core records. *American Journal of Science* **312**: 685–722.

Ridge JC, Bensonen MR, Brochu M *et al.* 1999. Varve, paleo-magnetic, and ^{14}C chronologies for Late Pleistocene events in New Hampshire and Vermont (U.S.A.); Late Quaternary history of the White Mountains, New Hampshire and adjacent southeastern Québec. *Geographie Physique et Quaternaire* **53**: 79–107.

Ridge JC, Toll NJ. 1999. Are late-glacial climate oscillations recorded in varves of the upper Connecticut Valley, northeastern United States?; International conference on recognition of abrupt climate change in clastic sedimentary environments; methods, limitations, and potential. *GFF* **121**: 187–193.

Stokes CR, Tarasov L, Dyke AS. 2012. Dynamics of the North American Ice Sheet Complex during its inception and build-up to the Last Glacial Maximum. *Quaternary Science Reviews* **50**: 86–104.

Tauxe L. 1993. Sedimentary records of relative paleointensity of the geomagnetic field: theory and practice. *Reviews of Geophysics* **31**: 319–354.

Thiel C, Buylaert J, Murray AS *et al.* 2011. Investigating the chronostratigraphy of prominent palaeosols in Lower Austria using post-IR IRSL dating. *Quaternary Science Journal* **60**: 137–152.

Ullman DJ, Carlson AE, LeGrande AN *et al.* 2015. Southern Laurentide ice-sheet retreat synchronous with rising boreal summer insolation. *Geology* **43**: 23–26.

Valen V, Lauritzen S, Lovlie R. 1997. Sedimentation in a high-latitude karst cave: Sirijordgrotta, Nordland, Norway. *Norsk Geologisk Tidsskrift* **77**: 233–250.

van der Meer JJM, Menzies J, Rose J. 2003. Subglacial till: the deforming glacier bed. *Quaternary Science Reviews* **22**: 1659–1685.

Ward B, Wilson M, Nagorsen D, *et al.* 2003. Port Eliza cave: North American West Coast interstadial environment and implications for human migrations. *Quaternary Science Reviews* **22**: 1383–1388.

Weremeichik J, Mylroie J. 2014. Glacial Lake Schoharie: an investigative study of glaciolacustrine lithofacies in caves, Helderberg Plateau, Central New York. *Journal of Cave and Karst Studies* **76**: 127–138.

Wood JR, Forman SL, Everton D *et al.* 2010. Lacustrine sediments in Porter Cave, Central Indiana, USA and possible relation to Laurentide Ice Sheet marginal positions in the middle and late Wisconsinan. *Palaeogeography Palaeoclimatology Palaeoecology* **298**: 421–431.

Wright SF. 2015. Late Wisconsinan ice sheet flow across northern and central Vermont, USA. *Quaternary Science Reviews* **129**: 216–228.